

Charge order in Fe_2OBO_3 : An LSDA + U study

I. Leonov¹, A. N. Yaresko², V. N. Antonov³, J. P. Atteld⁴, and V. I. Anisimov⁵

¹ Theoretical Physics III, Center for Electronic Correlations and Magnetism, Institute for Physics, University of Augsburg, Germany

² Max-Planck Institute for the Physics of Complex Systems, Dresden, Germany

³ Institute of Metal Physics, Vernadskii Street, 03142 Kiev, Ukraine

⁴ Centre for Science at Extreme Conditions, University of Edinburgh, Erskine, Williamson Building, King's Buildings, Mayfield Road, Edinburgh EH9 3JZ, United Kingdom and

⁵ Institute of Metal Physics, Russian Academy of Science-Ural Division, 620219 Yekaterinburg GSP-170, Russia
(Dated: March 23, 2024)

Charge ordering in the low-temperature monoclinic structure of iron oxoborate (Fe_2OBO_3) is investigated using the local spin density approximation (LSDA)+U method. While the difference between t_{2g} minority occupancies of Fe^{2+} and Fe^{3+} cations is large and gives direct evidence for charge ordering, the static "screening" is so effective that the total 3d charge separation is rather small. The occupied Fe^{2+} and Fe^{3+} cations are ordered alternately within the chain which is infinite along the a -direction. The charge order obtained by LSDA+U is consistent with observed enlargement of the β angle. An analysis of the exchange interaction parameters demonstrates the predominance of the interribbon exchange interactions which determine the whole L-type ferrimagnetic spin structure.

PACS numbers: 71.20.-b, 71.28.+d, 71.30.+h

I. INTRODUCTION

Transition metal compounds with interplay of spin, orbital, and charge degrees of freedom are of strong current interest. Thus, magnetite (Fe_3O_4), the famous lodestone,¹ is one of the classical examples of such a system, where a first-order metal-insulator transition occurs at 120 K.² According to Verwey this transition is caused by the ordering of Fe^{2+} and Fe^{3+} cations on the octahedral B-sublattice of the inverted spinel structure AB_2O_4 .^{3,4} Recently, the local spin density approximation (LSDA)+U method^{5,6,7} has been used for investigation of the low-temperature monoclinic structure^{8,9} of Fe_3O_4 .¹⁰ The charge and orbitally ordered insulating ground state with two different order parameters: small for the charge and large for the orbital order was obtained self-consistently. While the first order parameter was introduced as the total 3d charge separation between Fe^{2+} and Fe^{3+} cations, the latter one corresponds to the charge difference between occupancies of occupied $t_{2g\uparrow}$ orbital of Fe^{2+} and unoccupied $t_{2g\uparrow}$ orbital of Fe^{3+} cations. But an important issue, which is still unresolved is whether the charge ordering in magnetite is driven by Coulomb repulsion between the charges, or by the strain arising from electron-lattice interactions. An analysis of the charge and orbital order parameters¹⁰ in Fe_3O_4 inevitably results in a strong interplay between Jahn-Teller effect and electrostatic repulsion between electrons. Therefore, theoretical investigations of the isostructural iron and manganese oxoborate (Fe_2OBO_3 and Mn_2OBO_3 , correspondingly) that support predominantly electrostatic and Jahn-Teller distortion driven mechanism¹¹ behind the charge ordering in the same structural arrangement, are highly desirable.

Iron borate (Fe_2OBO_3) is a semi-valent oxide.^{12,13} It

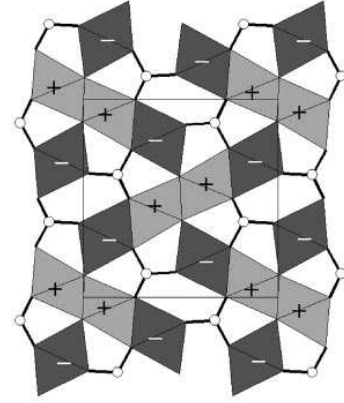


FIG. 1: The Fe_2OBO_3 structure projected on (100) plane (b vertical, c horizontal). Two structurally distinct $\text{Fe}(1)\text{O}_6$ and $\text{Fe}(2)\text{O}_6$ octahedra shown by light and dark shading respectively. Plus and minus signs indicate the relative orientation of the moments within each $\text{Fe}(1)$ and $\text{Fe}(2)$ chains in the magnetically ordered phase.

belongs to the homometallic warwickite family with formal chemical formula M^0BO_3 , where M and M^0 are, respectively, a divalent and trivalent metal ions. Surprisingly, that the homometallic ($\text{M} = \text{M}^0$) warwickites are known only for Fe ^{12,13} and Mn .^{14,15} In both compounds themetal have octahedral coordination. These octahedra share edges to form ribbons of four infinite along crystallographic a -direction chains of octahedra linked by corner sharing and the trigonal BO_3 groups (see Fig. 1).

There are two crystallographically inequivalent sites of the metal ions $\text{Fe}(1)$ and $\text{Fe}(2)$. Fe_2OBO_3 is L-type ferrimagnetic with drastically smaller in comparison to Fe_3O_4 critical temperature of $T_c \approx 155$ K, the $\text{Fe}(1)$ magnetic moments being aligned antiparallel to the

Fe(2) moments. It is almost antiferromagnetic but a small ferrimagnetic moment of $0.03 \mu_B$ per Fe atom in a 0.05 T field was found.^{11,12,13,16} At room temperature Fe_2O_3 is a semiconductor with a thermally activated conductivity $\sigma \propto e^{-E_a/kT}$ with $E_a = 0.35$ eV.^{11,12} Upon further heating a broad semiconductor-to-semiconductor transition occurs at $T_{co} = 317$ K, where resistivity drops down by a factor of 3, and, as a result, a small decreasing of the activated energy up to $E_a = 0.31$ eV above 350 K is observed.^{11,12} The 317 K transition is assigned to charge ordering of $2+$ and $3+$ Fe cations on Fe(1) and Fe(2) sites, and accompanied by a structural transition from monoclinic $P2_1/c$ to orthorhombic $Pmcn$ symmetry with increasing temperature. This structural transition is attributed by modification of the angle from $\beta = 90.220(1)$ at 3 K to $\beta = 90^\circ$ at 337 K.^{11,12,13} The change in conductivity and structure are small. But the ^{57}Fe Mossbauer spectra at around 317 K clearly result in the charge localization at the transition with an equal distribution of Fe^{2+} and Fe^{3+} cations over the two structurally distinct Fe(1) and Fe(2) sites with formal chemical formula $\text{Fe(1)}_{0.5}^{2+}\text{Fe(1)}_{0.5}^{3+}\text{Fe(2)}_{0.5}^{2+}\text{Fe(2)}_{0.5}^{3+}\text{O}_3$.^{11,12,13,16,17,18,19} Although, there are two types of distorted FeO_6 octahedra with Fe-O bond length varying between 1.92 and 2.23 Å for 3 K, the average Fe(1)-O and Fe(2)-O distances are 2.085 and 2.082 Å, respectively, i.e. equal within experimental errors.¹² Such a small difference results in the extremely small value of deviation (~ 0.01) from the average 2.5+ value of valence of Fe cations estimated by the bond valence sum method. While an electronic transition between charge ordered and disordered state occurs at around 317 K, as evidenced by Mossbauer spectroscopy and resistivity measurements, no long range $\text{Fe}^{2+}/\text{Fe}^{3+}$ ordering is directly observed by x-ray, neutron or electron diffraction. Thus, a long range charge ordering such as the simple alternating scheme proposed in Ref. 11 destroys the mirror symmetry, which leads to a tilting of the Fe-ribbons, consistent with the observed enlargement of the angle below the transition. However, there is no observation of the increasing of a-axis periodicity (it should increase by a factor of two or another integer factor below T_{co}). Thus, below the transition, a charge ordering is not implicit in the atom coordinates, although it is indirectly evidenced by other experiments. This ambiguity is resolved in our electronic structure study, which reveals an arrangement of Fe^{2+} and Fe^{3+} cations alternately ordered within the chains along the a-direction.

In this paper we report theoretical investigation of the electronic structure and magnetic properties of Fe_2O_3 in the low-temperature $P2_1/c$ structure. The LSDA+U approach in the tight-binding linear muffin-tin orbital (TB-LMTO) calculation scheme^{5,6} has been used. Motivated by our results, we propose an order parameter, defined as the difference between t_{2g} minority spin occupancies of Fe(1)^{2+} and Fe(1)^{3+} as well as the difference between t_{2g} majority spin occupancies of Fe(2)^{2+}

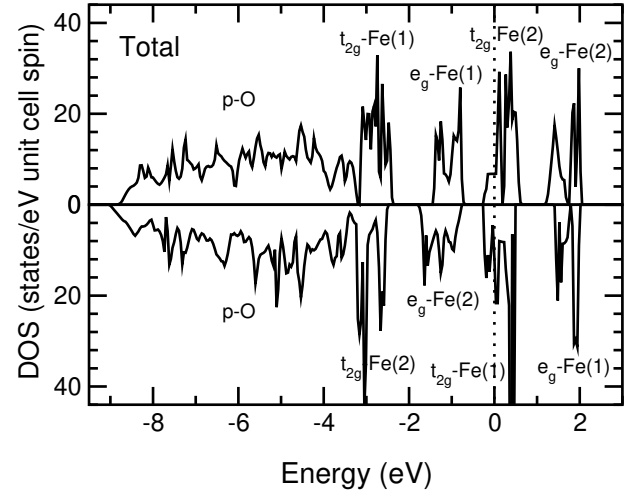


FIG. 2: Total density of states (DOS) obtained from the LSDA calculations for the low-temperature $P2_1/c$ phase of Fe_2O_3 . The Fermi level is shown by dotted line.

and Fe(2)^{3+} cations. This order parameter is found to be quite large, although the total 3d charge difference between $2+$ and $3+$ cations, is small.

II. COMPUTATIONAL DETAILS

The present band-structure calculations have been carried out for the low-temperature monoclinic structure of Fe_2O_3 . The corresponding $P2_1/c$ unit cell contains four Fe_2O_3 formula units. We used atom coordinates from Ref. 11 (see Table 1) and the cell parameters $a = 3.1688$ Å, $b = 9.3835$ Å, $c = 9.2503$ Å, and $\beta = 90.22^\circ$ refined at 3 K.^{11,12,13} The radii of muffin-tin spheres were taken $R_{\text{Fe}} = 2.5$ a.u., $R_{\text{O}} = 1.275$ a.u., $R_{\text{O1p04}} = 1.7$ a.u., and $R_{\text{O2p03}} = 1.8$ a.u. Seven kinds of empty spheres were introduced to fill up the interatomic space. For simplicity we neglect small spin-orbit coupling (for instance, in other iron oxide, in Fe_3O_4 , the spin-orbital interaction for 3d electrons was found to be negligibly small). We consider only a collinear spin case, in which the ferrimagnetic moments are aligned along the a-direction (see Table 1 of Ref. 13), which is in a reasonably good agreement with the experimental magnetic structure of Fe_2O_3 below T_c .

III. LSDA BAND STRUCTURE

The LSDA calculations give only a metallic ferrimagnetic solution without charge separation where partially filled bands at the Fermi level originate from the t_{2g} orbitals of Fe cations (see Fig. 2).

The lower part of the valence band (below -3.5 eV) is mainly formed by O 2p states with a bonding hybridization with Fe 3d states. Fe 3d states give predominant

contribution to the bands at -3.5 eV below and up to 2.5 eV above the Fermi level. The exchange splitting between the spin-up and spin-down Fe 3d states is roughly 3 eV. Additionally, the five-fold 3d levels are split by the crystal field into t_{2g} and e_g sub-bands. The oxygen octahedra in Fe_2OBO_3 are strongly distorted and the local symmetry of Fe sites is, of course, lower than cubic. Nevertheless, the cubic component of the ligand field, which is determined by the relative strength of Fe d- O p hybridization of π - and σ -type, remains dominant, whereas the splitting within " t_{2g} " and " e_g " subbands is smaller than the corresponding band width. This allows one to label the corresponding states as t_{2g} and e_g . The crystal field splitting is roughly 2 eV, which is less than the exchange splitting. This is consistent with the high-spin state of the Fe cations. The symmetry inequivalence of Fe(1) and Fe(2) sites leads to an inexact cancellation of magnetic moments and results in a small ferrimagnetic moment of $0.31 \mu_B$ per formula unit. The absolute values of magnetic moments obtained by LSDA are $3.54 \mu_B$ and $3.81 \mu_B$ for Fe(1) and Fe(2) sites, respectively.

Fe(1) and Fe(2) t_{2g} and e_g states with the opposite spin projections share nearly the same energy intervals. Thus, Fe 3d states between -3.5 and -2.0 eV originate predominantly from majority spin Fe(1) and minority spin Fe(2) t_{2g} states whereas the states between -2.0 and -0.5 eV are mainly of e_g character. Partially occupied bands crossing the Fermi level are formed by minority spin Fe(1) and majority spin Fe(2) t_{2g} states. The nominal occupation of these bands is $1/6$. In the majority spin channel, however, the Fe(2) t_{2g} state, that is oriented in the plane perpendicular to the shortest Fe(2)-O bond, forms quasi-one-dimensional bands with a strong dispersion along the a -direction. The one-dimensional character of the dispersion is explained by the fact that there are only two nearest neighbours of the same kind around each Fe(2) ion. The other two Fe(2) t_{2g} states are shifted to higher energy and the corresponding bands are completely unoccupied. As a result, the majority spin bands crossing the Fermi level turn out to be half-filled. An Fe(1) ion, in contrast to Fe(2) one, has four Fe(1) neighbours at close distances. As a result of the hybridisation between Fe(1) t_{2g} states the situation in the minority spin channel is more complicated. Twelve t_{2g} bands are split into three groups of 4 bands each. The Fermi level is crossed by lowest bands which show a rather strong dispersion along a -direction but with a period two times smaller than the quasi-one-dimensional Fe(2) bands.

It should be noted that in contrast to experimental data^{11,17,18} LSDA predicts Fe_2OBO_3 to be metallic with substantial magnetic moment per unit cell. Apparently, the electron-electron correlations, mainly in the 3d shell of Fe cations, play a significant role.

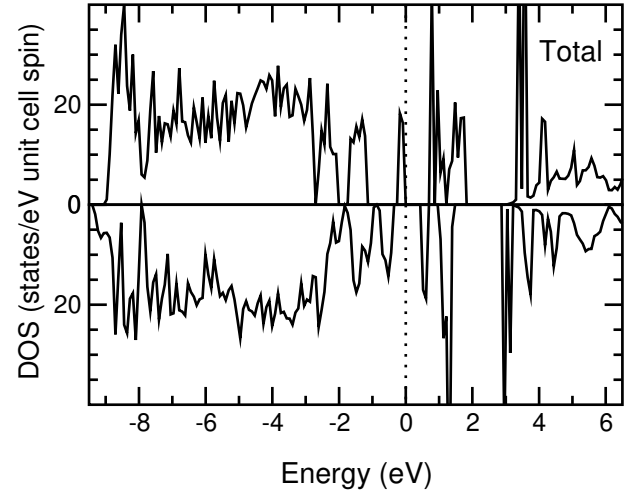


FIG. 3: The total DOS obtained from LSDA+U calculations with $U = 5.5$ eV and $J = 1$ eV for the low-temperature $P2_1/c$ phase of Fe_2OBO_3 . The top of the valence band is shown by dotted lines.

IV. LSDA+U RESULTS AND CHARGE ORDERING

To proceed further we take into account the strong electronic correlations in Fe 3d shell using the LSDA+U method. The calculations have been performed for the $P2_1/c$ unit cell as well as for double (2a b c) and triple (3a b c) $P2_1/c$ supercells of Fe_2OBO_3 (without putting in any additional local displacements of oxygen atoms around of $\text{Fe}^{2+}/\text{Fe}^{3+}$ sites). For the 2a b c supercell the LSDA+U calculations using the classical value of Coulomb ($U = 5$ eV) and exchange ($J = 1$ eV) interaction parameters for Fe result in an insulating charge ordered (CO) solution with an energy gap of 0.13 eV. This is in a strong contrast to metallic solution without CO obtained by the LSDA. The CO pattern obtained from the calculations is similar to the one proposed in Ref. 11. This is a notable result because the CO is not implicit in the atomic coordinates, and it shows that LSDA+U calculations can assist experiments in revealing CO arrangements. To obtain a reasonably good agreement of the calculated gap of 0.39 eV with experimental value of 0.35 eV we increase the U value up to 5.5 eV (see Fig. 3). It does not exceed of 10% of the U value, which is in an accuracy of the U calculation. Note, however, that the CO obtained by LSDA+U within 2a b c supercell does not depend on the U value of $5-5.5$ eV. Here and in the following all results are presented for the double along a -direction $P2_1/c$ supercell of Fe_2OBO_3 .

After self-consistency each of two groups of Fe(1) and Fe(2) atoms is split out in two subgroups of $2+$ and $3+$ Fe cations with equal number of $2+$ and $3+$ cations. Thus, one of t_{2g} majority/minority spin states of Fe(2)/Fe(1) atom becomes completely occupied, whereas all other t_{2g} states are pushed by strong Coulomb interaction at the

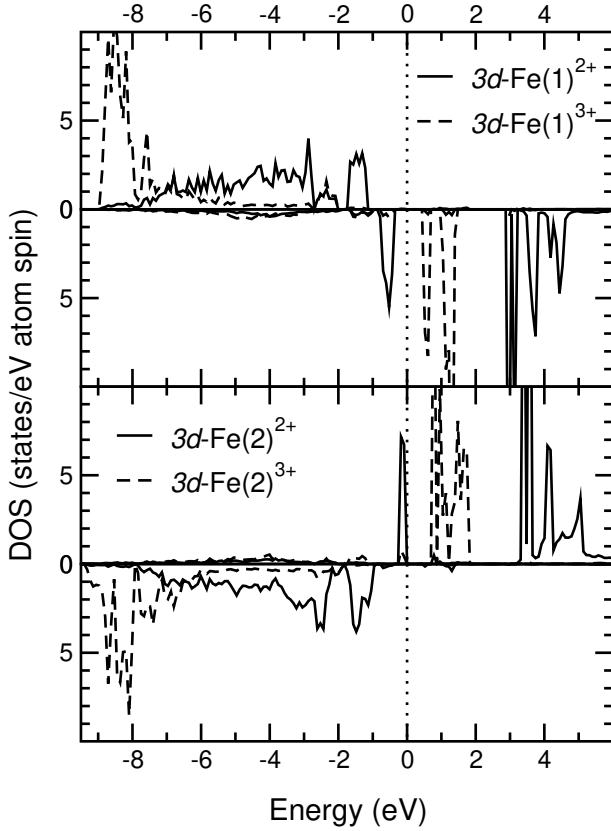


FIG. 4: The partial DOS for different Fe cations are shown. The gap is opened between $\text{Fe}(2)^{2+}$ and $\text{Fe}(2)^{3+}$ for a majority spin and $\text{Fe}(1)^{2+}$ and $\text{Fe}(1)^{3+}$ cations form minority spin states. The gap value of 0.39 eV was obtained by LSDA+U with $U = 5.5$ eV and $J = 1$ eV. The Fermi level is shown by dotted line.

energies above 3 eV. The gap is opened between occupied and unoccupied t_{2g} states of $\text{Fe}(1)^{2+}$ and $\text{Fe}(1)^{3+}$ for spin-down and $\text{Fe}(2)^{2+}$ and $\text{Fe}(2)^{3+}$ for spin-up. Majority spin 3d states of $\text{Fe}(1)^{3+}$ and minority spin states of $\text{Fe}(2)^{3+}$ cations are shifted below the O 2p states, which form the band in the energy range of -8 and -2 eV. In contrast to Fe^{3+} states, the majority spin $\text{Fe}(1)^{2+}$ and minority spin $\text{Fe}(2)^{2+}$ 3d states form the broad bands between -8 and -1 eV.

The obtained magnetic structure is almost antiferromagnetic (without spin moment per unit cell) with nearly the same spin moment per $\text{Fe}(1)^{2+}$ and $\text{Fe}(2)^{2+}$ as well as per $\text{Fe}(1)^{3+}$ and $\text{Fe}(2)^{3+}$ cations. Using the moment populations in Table I, the calculated net moment is 0.04 μ_B per Fe atom, in exact agreement with the experimental value (Ref. 11).

The charge order obtained by LSDA+U in 2a b c $P2_1=c$ supercell is consistent with observed enlargement of the angle below the transition and coincides with charge ordering scheme proposed earlier by Attfeld et al.: in 11. It is described by the sloping 2+ and 3+ Fe cation lines alternately stacked along a-direction, and could be considered as a quasiohedral dimensional analog of the Ver-

wey CO model in the pyrochlore lattice of Fe_3O_4 . Using the same U and J values we perform additional self-consistent LSDA+U calculations for $P2_1=c$ unit cell as well as for double and triple along a-direction $P2_1=c$ supercells. But only self-consistent solutions with larger value of the total energy or with substantial magnetic moment per unit cell, which contradicts to the experimental data, were found. Also we found that other charge arrangements in 2a b c $P2_1=c$ supercell are unstable, and the stable one coincides with the CO found previously. Thus, the CO obtained for certain value of U and J does not depend on the initial charge arrangement. It is not possible to check all possible CO arrangements including more complex CO scenarios, but our results consistently indicate that the obtained CO solution is more favourable than other simple alternatives, and is the ground state of Fe_2OBO_3 in the low-temperature phase.

Because of the small monoclinic distortion of the low temperature $P2_1=c$ structure the distances between the nearest Fe(1) cations become slightly different. It is important to note that in the calculated CO pattern the shortest (2.957 Å) is the distance between the pairs of equally charged Fe(1) cations whereas the distance between $\text{Fe}(1)^{2+}$ and $\text{Fe}(1)^{3+}$ cations turns out to be larger (2.961 Å). On the contrary, the pairs of Fe(1) and Fe(2) sites with the shortest distance between them are occupied by the cations of different valency. Thus, assuming a simple ionic model with the Coulomb interaction between Fe ions only the obtained CO pattern contradicts to the requirement of the minimal electrostatic energy. Indeed, the comparison of the Madelung energies shows that the energy lowers (about 0.07 eV per unit cell) if the nearest Fe(1) sites are occupied by $\text{Fe}(1)^{2+}$ and $\text{Fe}(1)^{3+}$ ions. This observation suggests that electron-lattice coupling rather than electrostatic repulsions drives the charge ordering in Fe_2OBO_3 ; the same conclusion was found for the charge order in Fe_3O_4 .^{8,9,10}

Although the corresponding total 3d charges difference (0.34e) and disproportion of the total electron charges inside the atomic spheres of Fe^{2+} and Fe^{3+} cations (0.24e) is small, an analysis of occupation matrices of 3d $\text{Fe}(1)/\text{Fe}(2)$ minority/majority spin states confirms substantial charge separation. Thus, as shown in Table I, one of the t_{2g} states of $\text{Fe}(1)^{2+}$ and $\text{Fe}(2)^{2+}$ cations is almost completely filled with the occupation numbers $n \approx 0.9$, whereas the remained two t_{2g} orbitals of the Fe^{2+} cations have significantly smaller population of about 0.1. According to Ref. 10 we define an order parameter as the largest difference between Fe^{2+} and Fe^{3+} t_{2g} populations. While due to strong static "screening" effects,²⁰ the order parameter introduced as the total 3d charge difference between 2+ and 3+ Fe cations is ill-defined, the well-defined order parameter is the difference of t_{2g} occupancies for Fe^{3+} and Fe^{2+} cations, which amounts to 80% of ideal ionic CO model and clearly pronounces the existence of CO below the transition. The occupation matrices analysis shows that the change of the t_{2g} occupations caused by the charge ordering is very effectively screened by the

TABLE I: Total and l-projected charges, magnetic moments, and occupation of the most populated t_{2g} orbitals calculated for inequivalent Fe atoms in the low-temperature $P2_1/c$ phase of Fe_2OBO_3 .

Fe ion	q	q_s	q_p	q_d	M (B)	t_{2g} orbital	n
$\text{Fe}(1)^{3+}$	6.90	0.40	0.55	5.95	-4.20	—	0.10
$\text{Fe}(1)^{2+}$	7.12	0.35	0.50	6.27	-3.65	d_{xy}	0.91
$\text{Fe}(2)^{3+}$	6.79	0.38	0.54	5.86	4.33	—	0.09
$\text{Fe}(2)^{2+}$	7.04	0.34	0.50	6.21	3.69	d_{xy}	0.89

TABLE II: The averaged Fe-O distances in the plane of t_{2g} orbitals for $P2_1/c$ structure of Fe_2OBO_3 . d_{xy} approximates to the doubly-occupied orbital of the $3d^6 \text{Fe}^{2+}$ states.

Fe atom	orbital	d_{orb} (Å)	d_{av} (Å)
Fe(1)	d_{xy}	2.111	2.085
	d_{yz}	2.076	
	d_{zx}	2.069	
Fe(2)	d_{xy}	2.109	2.082
	d_{yz}	2.083	
	d_{zx}	2.055	

rearrangement of the other Fe electrons. Thus, significant contribution to the charge screening is provided by $\text{Fe } e_g$ states due to relatively strong bonds with $2p \text{ O}$ states and, as a result, appreciable contribution to the occupied part of the valence band.

The occupied t_{2g} states of Fe^{2+} cations are predominantly of d_{xy} character in the local cubic frame (according to that we later mark the orbitals as d_{xy} orbital). This is illustrated in Fig. 5, which shows the angular distribution of the majority and minority spin 3d electron density of the $\text{Fe}(2)$ and $\text{Fe}(1)$ cations, respectively.²¹ Thus, occupied Fe^{2+} and unoccupied Fe^{3+} cations are ordered alternately within the chain which is infinite along a-direction. The angular distribution of charge density of the $\text{Fe}(1)$ and $\text{Fe}(2)$ cations, which correspondingly belongs to different Fe-ribbons being formed a cross in the Fe_2OBO_3 structure projected on (100) plane (see Fig. 1) is shown in Fig. 6. An analysis of interatomic distances (Table II) shows that the average $\text{Fe}(2)\text{-O}$ distance (2.109 Å) in the plane perpendicular to one of the diagonals of the distorted $\text{Fe}(2)\text{O}_6$ octahedron is considerably larger than average distances in the other two planes (2.055 and 2.083 Å). It turns out that the occupied $\text{Fe}(2)$ t_{2g} majority spin orbital is the one oriented in the plane with the largest average $\text{Fe}(2)\text{-O}$ distance. The same is also true for the $\text{Fe}(1)$ ion but in this case the variation of the average $\text{Fe}(1)\text{-O}$ distances is smaller (2.111 vs 2.069 and 2.076 Å) and, as a consequence, the out-of-plane rotation of the occupied t_{2g} minority spin orbital is stronger.

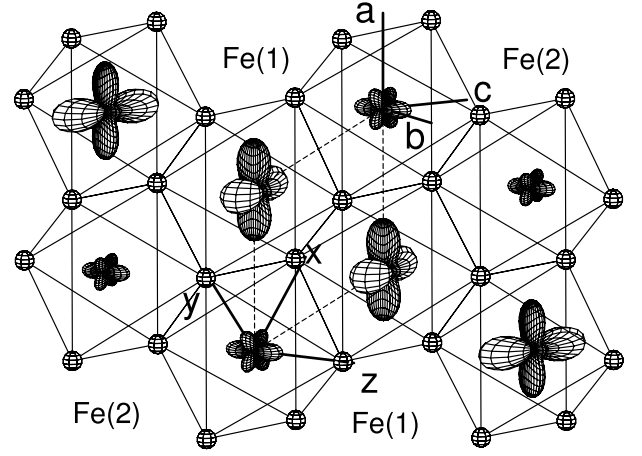


FIG. 5: The angular distribution of the majority and minority spin 3d electron density of the $\text{Fe}(2)$ and $\text{Fe}(1)$ cations, respectively, within Fe-ribbon. The size of orbital corresponds to its occupancy. Oxygen atoms are shown by small spheres. X-Y-Z coordinate system corresponds to the local cubic frame.

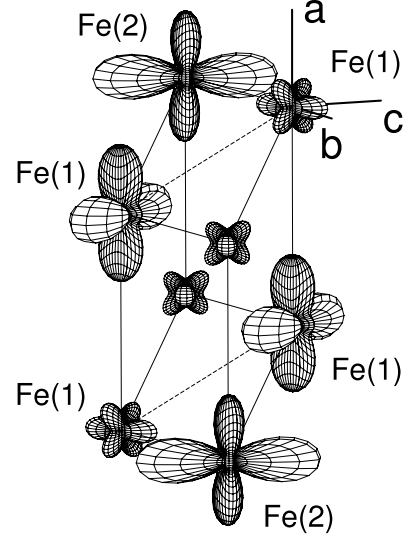


FIG. 6: The angular distribution of the majority and minority spin 3d electron density of the $\text{Fe}(2)$ and $\text{Fe}(1)$ cations, respectively, from different Fe-ribbons.²¹ The size of orbital corresponds to its occupancy. The frame of four $\text{Fe}(1)$ atoms from the Fe-ribbon presented in Fig. 5 is shown by dashed lines.

V. EXCHANGE COUPLING CONSTANTS

Using the LSDA+U method the exchange interaction parameters have been calculated via the variation of ground state energy with respect to the magnetic moment rotation angle.^{6,7} In Table III we have shown the total set of different intraribbon exchange parameters as well as a contribution of different subbands into exchange interactions. J_i represents the effective pair exchange interaction between Fe atoms with effective Heisenberg

TABLE III: Total and partial intraribbon exchange interaction parameters are shown. The values are given in kelvin. The spatial representation of all these exchanges is schematically presented in Fig. 7.

J_i	t_{2g}	t_{2g}	t_{2g}	e_g	e_g	e_g	Total
J_1	4		-22		-20		-38
J_2	-7		-38		1		-44
J_3	3		-19		-16		-32
J_4	4		-72		-1		-70
J_5	17		-69		-16		-69
J_6	53		-34		-13		6
J_7	-1		-11		-4		-16
J_8	-13		-120		-4		-136
J_9	3		-22		-20		-39

TABLE IV: Total and partial interribbon exchange interaction parameters are shown. The values are given in kelvin. The spatial representation of all these exchanges is schematically presented in Fig. 8.

J_i	t_{2g}	t_{2g}	t_{2g}	e_g	e_g	e_g	Total
J_{10}	-12		-114		-104		-229
J_{11}	-16		-140		-28		-183
J_{12}	-17		-141		-52		-209
J_{13}	-3		-52		-2		-56
J_{14}	-22		-165		-20		-207
J_{15}	-12		-115		-19		-147

Hamiltonian $H = \sum_{i>j} J_{ij} \mathbf{e}_i \cdot \mathbf{e}_j$, where \mathbf{e}_i and \mathbf{e}_j are magnetic moment unit vectors at site i and j . Positive (negative) values of J correspond to the ferromagnetic (antiferromagnetic) coupling between Fe sites. The spatial representation of all these exchanges is schematically presented in Fig. 7. Surprisingly, only the exchange interaction parameter between $\text{Fe}(2)^{2+}$ and $\text{Fe}(2)^{3+}$ cations is ferromagnetic with relatively small value of $J_6 = 6$ K. In contrast, the nearest sites in quasi-one-dimensional Fe(1) chain are coupled antiferromagnetically with noticeably larger exchange absolute value of $|J_5| = 69$ K. Furthermore, the exchange parameters between the nearest sites of two Fe(1) chains are relatively strong and antiferromagnetic (see J_2 , J_4 , and J_8 in Table III). Therefore, the Fe(1) sublattice is highly frustrated, while the relatively weak frustrations in the Fe(2) sublattice considerably reduce ferromagnetic interaction within Fe(2) chain. Also it is interesting to note that relatively strong ferromagnetic intrachain interaction between t_{2g} subbands of $\text{Fe}(2)^{2+}$ and $\text{Fe}(2)^{3+}$ cations (see J_6 in Table III) is strongly suppressed by the substantial antiferromagnetic $t_{2g} \{ e_g \}$ and $e_g \{ e_g \}$ exchange.

On the other hand, the interribbon exchange interaction parameters between Fe(1) and Fe(2) atoms are considerably larger. The values of these interactions are shown in Table IV, whereas the spatial representation is schematically presented in Fig. 8. Thus, the exchange parameters between $\text{Fe}(1)^{3+}$ and $\text{Fe}(2)^{2+}$ cations are antiferromagnetic with values of $J_{10} = -229$ K and $J_{14} = -$

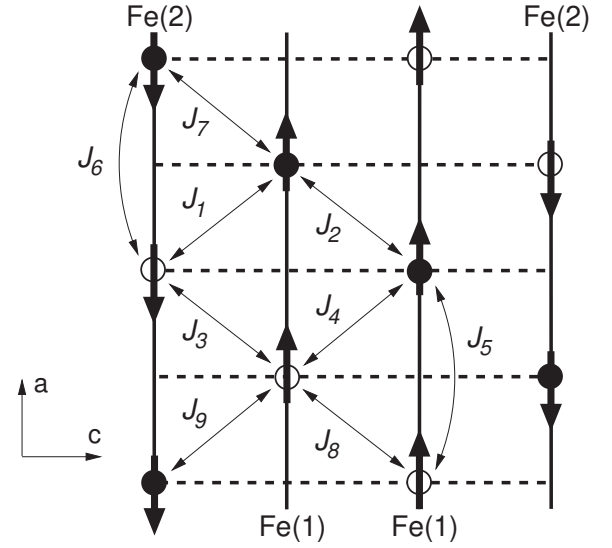


FIG. 7: The sketch of the arrangement of exchange interaction parameters within the ribbon of iron atoms. Open circles correspond to Fe^{3+} , while Fe^{2+} cations are noted by the closed circles. The spin moment direction on each Fe site is shown by an arrow.

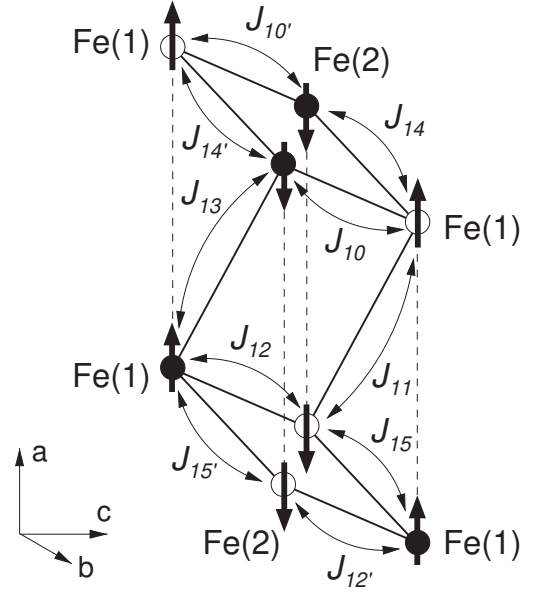


FIG. 8: The sketch of the arrangement of interribbon exchange interaction parameters. Open circles correspond to Fe^{3+} , while Fe^{2+} cations are noted by the closed circles. The spin moment direction on each Fe site is shown by arrow. Note that J_{i0} exchange parameters presented here have the same total values as J_i , while subband contributions are different.

207 K (see Table IV). Such an appreciable difference between J_{10} and J_{14} arises from geometry since the former is due to the superexchange interaction between Fe ions linked by shortest bonds to a common O ion. It seems that the geometrical reason is also responsible for

decreasing of absolute value of the exchange interactions between $\text{Fe}(1)^{2+}$ and $\text{Fe}(2)^{3+}$ cations from $J_{12} = 209$ K to $J_{15} = 147$ K (see Table IV). Also it is interesting to note that the exchange interaction between $\text{Fe}(1)^{3+}$ and $\text{Fe}(2)^{3+}$ cations is considerably larger than between $\text{Fe}(1)^{2+}$ and $\text{Fe}(2)^{2+}$ (J_{11} and J_{13} , respectively). We find that the interribbon exchange interactions play predominant role and determine the whole L-type ferrimagnetic spin structure below T_c in contrast to the ferromagnetic intrachain order due to $d^5 \{ d^6 \}$ superexchange.^{11,12}

VI. SUMMARY AND CONCLUSIONS

In summary, in the present LSDA+U study of the low-temperature $P2_1/c$ phase of Fe_2OBO_3 we found a charge ordered insulator with an energy gap of 0.39 eV. While the screening of the charge disproportion is so effective that the total 3d charge separation is rather small (0.34), the charge order is well pronounced with an order parameter defined as a difference of t_{2g} occupancies of 2+ and 3+ Fe cations (0.8). The occupied Fe^{2+} and Fe^{3+} cations are ordered alternately within infinite along a -axis chains of Fe atoms. This result is remarkable in view of the absence of directly observed CO atomic displacements in the experimental coordinates, and demonstrates the utility of the LSDA+U method as an aide to exper-

imental studies of CO structures. However, the charge order obtained by LSDA+U is consistent with observed enlargement of the c angle and coincides with charge ordering scheme proposed earlier by Attfeld et al.¹¹ It seems certain that Fe_2OBO_3 is charge ordered below T_{co} , and the absence of the long range charge ordering from x-ray, neutron or electron diffraction arises from formation of charge order within small domains, which have been termed "Wigner nanocrystals".²² Thus, the superstructure peaks are too weak and broad to be observed against background in diffraction patterns, whereas the observed long range monoclinic lattice distortion can arise despite a large concentration of defects as these preserve the direction of the monoclinic distortion, but do not propagate the coherent doubling of the lattice periodicity. An analysis of the exchange interaction parameters obtained by LSDA+U method inevitably results in predominance of the interribbon exchange interactions which determine the whole L-type ferrimagnetic spin structure below T_c , in contrast to the ferromagnetic intrachain order due to $d^5 \{ d^6 \}$ superexchange proposed earlier in Ref. 11.

We are grateful to M. A. Korotin, R. Claessen, P. Fulde, and D. Vollhardt for helpful discussions. The present work was supported in part by RFFI Grant No. 04-02-16096, No. 03-02-39024, and by the Sonderforschungsbereich 484 of the Deutsche Forschungsgemeinschaft (DFG).

- ¹ D. C. Mattis: The Theory of Magnetism I (Springer, Berlin 1988)
- ² Several reviews of research on the Verwey transition up to 1980 are contained in the special issue of Philos. Mag. B 42 (1980).
- ³ E. J. W. Verwey, Nature (London) 144, 327 (1939).
- ⁴ E. J. W. Verwey, P. W. Haayman, and F. C. Romijn, J. Chem. Phys. 15, 181 (1947).
- ⁵ V. I. Anisimov, J. Zaanen, and O. K. Andersen, Phys. Rev. B 44, 943 (1991).
- ⁶ A. I. Lichtenstein, V. I. Anisimov, and J. Zaanen, Phys. Rev. B 52, 5467 (1995).
- ⁷ V. I. Anisimov, F. Aryasetiawan, and A. Lichtenstein, J. Phys.: Condens. Matter 9, 767 (1997).
- ⁸ J. P. Wright, J. P. Attfeld, and P. G. Radaelli, Phys. Rev. Lett. 87, 266401 (2001).
- ⁹ J. P. Wright, J. P. Attfeld, and P. G. Radaelli, Phys. Rev. B 66, 214422 (2002).
- ¹⁰ I. Leonov, A. N. Yaresko, V. N. Antonov, M. A. Korotin, and V. I. Anisimov, Phys. Rev. Lett. 93, 146404 (2004).
- ¹¹ J. P. Attfeld, A. M. T. Bell, L. M. Rodriguez-Martinez, J. M. G. Renche, R. J. Cemik, J. F. Clarke, and D. A. Perkins, Nature 396, 655 (1998).
- ¹² J. P. Attfeld, A. M. T. Bell, L. M. Rodriguez-Martinez, J. M. G. Renche, R. Retoux, M. Leblanc, R. J. Cemik, J. F. Clarke, and D. A. Perkins, J. Mater. Chem. 9, 205 (1999).
- ¹³ J. P. Attfeld, J. F. Clarke, and D. A. Perkins, Physica B 180-181, 581 (1992).
- ¹⁴ R. J. Go, A. J. Williams, and J. P. Attfeld, Phys. Rev. B 70, 014426 (2004).
- ¹⁵ R. Norrestam, M. Krikos, and A. Sjödin, J. Solid State Chem. 144, 311 (1995).
- ¹⁶ M. A. Continentino, A. M. Pedreira, R. B. Guimarães, M. Mir, J. C. Fernandes, R. S. Freitas, and L. Ghivelder, Phys. Rev. B 64, 014406 (2001).
- ¹⁷ A. P. Douvalis, V. Papaefthymiou, A. M. Oukarika, T. Bakas, and G. Kallias, J. Phys.: Condens. Matter 12, 177 (2000).
- ¹⁸ A. P. Douvalis, V. Papaefthymiou, A. M. Oukarika, and T. Bakas, Hyperfine Interactions 126, 319 (2000).
- ¹⁹ N. Suda, K. Kohn, and S. Nakamura, Ferroelectrics 286, 155 (2003).
- ²⁰ Here and in the following we assume a redistribution of charge between $\text{Fe } t_{2g}$ and other states using term screening.
- ²¹ The distribution is calculated according to $\langle n_{m\sigma} \rangle = \frac{1}{Z} \text{Tr} [n_{m\sigma} e^{-\beta H}]$, where $n_{m\sigma}$ is the occupation matrix of 3d minority states of $\text{Fe}(1)$ and 3d majority states of $\text{Fe}(2)$ cations. The occupation matrices were calculated by the LSDA+U with $U = 5.5$ eV, $J = 1$ eV for the low-temperature $P2_1/c$ phase of Fe_2OBO_3 . $Y_m(\sigma)$ are corresponding spherical harmonics.
- ²² G. K. H. Rozenberg, G. R. Heame, M. P. Pasternak, P. A. M. et al., and J. M. Honig Phys. Rev. B 53, 6482 (1996).